THE JOURNAL OF BIOLOGICAL CHEMISTRY VOL. 286, NO. 30, pp. 26794–26805, July 29, 2011

Conditional Inactivation of the CXCR4 Receptor in Osteoprecursors Reduces Postnatal Bone Formation Due to Impaired Osteoblast Development*

Received for publication, April 13, 2011, and in revised form, June 1, 2011 Published, JBC Papers in Press, June 2, 2011, DOI 10.1074/jbc.M111.250985

Wei Zhu[‡§1], **Gang Liang**[‡], **Zhiping Huang**[‡], **Stephen B. Doty**[‡], **and Adele L. Boskey**[‡¶]

From the [‡]*Musculoskeletal Integrity Program, Hospital for Special Surgery, New York, New York 10021 and the Departments of* [§]*Cell and Developmental Biology and* [¶]*Biochemistry, Weill Cornell Medical College, New York, New York 10021*

Cysteine (C)-*X*-C motif chemokine receptor 4 (CXCR4), the primary receptor for stromal cell-derived factor-1 (SDF-1), is involved in bone morphogenic protein 2 (BMP2)-induced osteogenic differentiation of mesenchymal progenitors. To target the *in vivo* function of CXCR4 in bone and explore the underlying mechanisms, we conditionally inactivated CXCR4 in osteoprecursors by crossing osterix (Osx)-Cre mice with floxed CXCR4 (CXCR4$^{fl/fl}$) mice to generate knock-outs with CXCR4 deletion driven by the Osx promoter (*Osx*::*CXCR4*$^{fl/fl}$). The Cre-mediated excision of CXCR4 occurred exclusively in bone of *Osx*::*CXCR4*$^{fl/fl}$ mice. When compared with littermate controls, *Osx*::*CXCR4*$^{fl/fl}$ mice developed smaller osteopenic skeletons as evidenced by reduced trabecular and cortical bone mass, lower bone mineral density, and a slower mineral apposition rate. In addition, *Osx*::*CXCR4*$^{fl/fl}$ mice displayed chondrocyte disorganization in the epiphyseal growth plate associated with decreased proliferation and collagen matrix syntheses. Moreover, mature osteoblast-related expression of type I collagen α1 and osteocalcin was reduced in bone of *Osx*::*CXCR4*$^{fl/fl}$ mice *versus* controls, suggesting that CXCR4 deficiency results in arrested osteoblast progression. Primary cultures for osteoblastic cells derived from *Osx*::*CXCR4*$^{fl/fl}$ mice also showed decreased proliferation and impaired osteoblast differentiation in response to BMP2 or BMP6 stimulation, and suppressed activation of intracellular BMP receptor-regulated Smads (R-Smads) and Erk1/2 was identified in CXCR4-deficient cells and bone tissues. These findings provide the first *in vivo* evidence that CXCR4 functions in postnatal bone development by regulating osteoblast development in cooperation with BMP signaling. Thus, CXCR4 acts as an endogenous signaling component necessary for bone formation.

Cysteine (C)-*X*-C motif chemokine receptor 4 (CXCR4)[2] is the primary transmembrane receptor for signaling chemokine stromal cell-derived factor-1 (SDF-1; also named CXCL12 or pre-B cell stimulating factor) (1–4). Both CXCR4 and SDF-1 are highly conserved in various mammalian cell types and have broad functions in cell proliferation, morphogenesis, and migration. The CXCR4$^{-/-}$ and SDF-1$^{-/-}$ mice die *in utero* or perinatally due to multiple defects in developing brain, heart, vasculature, intestine, and hematopoietic tissues (5–7). Mutations at the carboxyl terminus of CXCR4 gene also lead to the warts, hypogammaglobulinemia, infections, and myelokathexis syndrome in humans, a complex immunodeficiency disease associated with neutropenia and defective B cell development (8). The binding of SDF-1 to CXCR4 induces cytoskeleton rearrangement and integrin activation and eventually results in the migration of CXCR4-expressing cells toward high gradients of SDF-1 (9–16). This SDF-1/CXCR4-mediated chemotaxis is involved in a variety of physiological and pathological events including blood homeostasis (9), cellular inflammatory and immune response (10), bone remodeling (11), homing of stem/progenitor cells to bone marrow reservoir (17), tumor metastasis to bone or other organs containing high levels of SDF-1 (18), and cell recruitment in injured tissues (15, 19–24).

Previous studies suggested the expression of CXCR4 and SDF-1 in bone; however, their direct function as well as underlying mechanisms remained poorly defined. This is probably due to the absence of demonstrable reports about skeletal abnormalities in patients with CXCR4 mutations or mice lacking CXCR4 or SDF-1. In fact, accumulating evidence has suggested the intimate association of the SDF-1/CXCR4 pathway with progenitor cells that have potentials to become bone-producing osteoblasts or form bone. Expression of SDF-1 and CXCR4 is found in both mesenchymal cell cultures (15, 21, 25, 27) and bone sections (28–32) with greater levels in less differentiated cells or immature osteoblasts relative to mature osteoblasts and osteocytes. High levels of SDF-1 are also present in regions of perichondrium of embryonic bones and periosteum of injured bones where osteoprogenitors arise and differentiate (15, 28–32). In addition, retrovirus-mediated overexpression of SDF-1 in human mesenchymal stem cells was found to enhance

* This work was supported, in whole or in part, by National Institutes of Health Grant AR046121 from the NIAMS-funded Musculoskeletal Repair and Regeneration Core Centers. This work was also supported by grants from the Arthritis Foundation and Beatrice and Samuel A. Seaver Foundation.

[1] To whom correspondence should be addressed: Hospital for Special Surgery, Caspary Research Bldg., Rm. 624, 535 East 70th St., New York, NY 10021. Tel.: 212-774-7017; Fax: 212-774-7877; E-mail: zhuw@hss.edu.

[2] The abbreviations used are: CXCR4, cysteine (C)-*X*-C motif chemokine receptor 4; SDF-1, stromal cell-derived factor-1; BMP, bone morphogenic protein; R-Smads, BMP receptor-regulated Smads; Osx, osterix; ProCol1α1, proform of type I collagen α1; Col2α1, type II collagen α1; Col10α1, type X collagen α1; PCNA, proliferating cell nuclear antigen; ALP, alkaline phosphatase; OCN, osteocalcin; CXCR4$^{fl/fl}$, floxed CXCR4; rh, recombinant human; μCT, microcomputed tomography; MAR, mineral apposition rate; qPCR, quantitative real time PCR; Bis-Tris, 2-[bis(2-hydroxyethyl)amino]-2-(hydroxymethyl)propane-1,3-diol; BV/TV, bone volume fraction (bone volume/tissue volume); Ct.Th, cortical thickness; BMD, bone mineral density; p, phosphorylated; fl, floxed.

mesenchymal stem cell induction of ectopic bone formation in nude mice (27). In mesenchymal cultures, such as human and mouse bone marrow-derived stromal cells (33) and C2C12 and ST2 cells (25), we demonstrated that blocking the SDF-1/CXCR4 signal axis inhibits the differentiation of these cells toward the osteoblastic lineage in response to bone morphogenic protein 2 (BMP2) stimulation. This reveals the direct involvement of the SDF-1/CXCR4 pathway in osteogenic differentiation *in vitro*. Moreover, recent evidence showing the effect of CXCR4 and SDF-1 on enhancing chondrocyte hypertrophy at the chondro-osseous junction of long bone further implicates the involvement of SDF-1 signaling in endochondral ossification (34). In light of these findings, we hypothesized that SDF-1 signaling functions in bone formation by affecting osteoblast development.

To address the direct role of SDF-1 signaling in bone formation *in vivo*, in this study, we used the Cre/loxP genetic approach to conditionally remove CXCR4 from osteoblastic lineage precursors under the control of an osterix (Osx) promoter. Osx (35) is a zinc-finger domain-containing transcription factor, downstream of Runx2, mainly expressed by osteoprecursors during early phases of osteogenic differentiation. Osx is considered one of the "master" regulators for bone formation, because $Osx^{-/-}$ mice (35), like $Runx2^{-/-}$ mice (36, 37), develop no bone in their skeletons. Using this Osx-controlled conditional deletion of CXCR4, we demonstrated the requirement for CXCR4 in bone formation of the mouse skeleton. Moreover, we identified the function of CXCR4 in regulating osteoblast activities and the interaction of CXCR4 with BMP signaling in this process.

EXPERIMENTAL PROCEDURES

Antibodies and Reagents—Anti-CXCR4 and anti-Osx antibodies were purchased from eBioscience (San Diego, CA) and Abcam (Cambridge, MA), respectively. Antibodies for type X collagen α1 (Col10α1), ProCol1α1, and proliferating cell nuclear antigen (PCNA) were purchased from the Developmental Studies Hybridoma Bank (University of Iowa, Iowa City, IA). Anti-osteocalcin (OCN) was purchased from Millipore (Billerica, MA). Antibodies for Smad1/5/8, phosphorylated Smad1/5, total Erk, phosphorylated Erk1/2, and β-tubulin were obtained from Cell Signaling Technology (Danvers, MA). Anti-phosphorylated Smad2 was purchased from Rockland Immunochemicals (Gilbertsville, PA). Antibodies for SDF-1, Col2α1, isotype-matched control antibodies, and secondary goat, sheep, or rabbit IgGs were from Santa Cruz Biotechnology (Santa Cruz, CA). Recombinant human (rh) BMP2 and BMP6 proteins were purchased from R&D Systems (Minneapolis, MN). General chemicals were from Sigma. All cell culture media and supplements were from Invitrogen.

Animals and Genotyping—All animal experiments were carried out following review and approval by the Institutional Animal Care and Use Committee at The Hospital for Special Surgery. $CXCR4^{fl/fl}$ mice (38–40), in which CXCR4 gene is flanked by loxP sequences, were provided by Dr. Yong-Rui Zou (Columbia University, New York, NY). Osx-Cre mice (41, 42), in which the expression of a tetracycline (Tet)-Off regulatable GFP-Cre fusion protein is transcriptionally controlled by an *Osx* promoter, were purchased from The Jackson Laboratory (Bar Harbor, ME). These two strains were crossed and maintained on a C57BL/6J background. We first generated double heterozygous mice for Cre and floxed CXCR4 (*Osx-Cre*; $CXCR4^{fl/+}$) that were then bred to $CXCR4^{fl/fl}$ mice via a backmating strategy to generate excised floxed CXCR4 homozygous (*Osx*::$CXCR4^{fl/fl}$; used as conditional knock-outs), heterozygous for floxed CXCR4 (*Osx-Cre*;$CXCR4^{fl/+}$), and Cre-null mice ($CXCR4^{fl/+}$ and $CXCR4^{fl/fl}$; used as littermate controls throughout the study). These mice were born at the expected Mendelian frequency. As additional controls, *Osx*::$CXCR4^{fl/fl}$ mice were fed with 200 μg/ml doxycycline (tetracycline analog; Sigma) in drinking water, which prevents the *Osx* promoter from driving *Cre* expression, as suggested by the manufacturer.

For genotyping, genomic DNA was isolated from tail tips using the DNeasy Blood and Tissue kit (Qiagen, Valencia, CA). PCRs were performed using PCR Master Mix (Fermentas, Glen Burnie, MD) with primer sequences for *Cre* transgene and floxed *Cxcr4* gene relative to wild type *Cxcr4* as shown in Table 1.

X-ray and Microcomputed Tomography (μCT) Analyses—For skeletal analysis, mice were sacrificed by CO_2 inhalation, and x-rays (40 kV, 4 mA·s, source to image receptor distance of 130 cm; Faxitron, Lincolnshire, IL) were obtained in both lateral and anterior-posterior views to assess the spinal length and the femoral/tibial length, respectively, in the mouse skeleton.

μCT (Scanco Medical MicroCT 35) was performed on both calvariae and tibiae of mice. Entire calvariae and tibiae were scanned (isotropic resolution of 15–20 μm) to obtain grayscale images, which were Gaussian-filtered and globally thresholded (15.2% of maximum gray value) to form binarized images for morphological analyses. Quantitative volumetric analyses of cortical and trabecular microstructures were performed on entire parietal calvariae and on a region of 200 microtomographic slices (2.1 mm) at the proximal tibia with an isotropic resolution of 6 μm. These analyses measured the cortical and trabecular bone volume fraction, thickness, and bone mineral density as well as trabecular number, separation, and connectivity density.

Double Fluorochrome Labeling and Mineral Apposition Rate (MAR)—To measure bone mineralization *in vivo*, mice were subcutaneously and sequentially injected with xylenol orange (orange-red) and tetracycline (green) at 20 μg/g (body weight) each in a 4-day time interval. One day after the second injection, tibiae were collected, fixed in 80% ethanol, then subjected to poly(methyl methacrylate) embedding, and sectioned to 8–10 μm.

Histomorphometry analysis using OsteoII software (Bioquant, Nashville, TN) was performed on tibia sections to measure the distance between two fluorochrome-labeled mineralization fronts at the midshaft of tibia. Periosteal MAR was calculated by dividing the measured distance by the time interval.

Histology, Immunohistochemistry, and Histomorphometry—For phenotypic analysis, tibiae including knee joints or calvariae were fixed in sodium phosphate-buffered 4% paraformaldehyde at 4 °C for 2–4 days, decalcified in 5% EDTA, and transferred to 70% ethanol until paraffin wax embedding. These

TABLE 1
Primer sequences used in RT-PCR and qPCR

Target gene	GenBank accession no.	Sequences (5′–3′)	Product size
			bp
Cre recombinase	HQ335171	Forward, GCGGTCTGGCAGTAAAAACTATC; reverse, GTGAAACAGCATTGCTGTCACTT	102
Floxed *Cxcr4 vs. Cxcr4*	U65580	Forward, CACTACGCATGACTCGAAATG; reverse, GTGTGCGGTGGTATCCAGC	434 *vs.* 334
Cxcr4	NM_009911	Forward, GATAGCCTGTGGATGGTGGT; reverse, GCAGGCAAAGAAAGCTAGGA	180
Osx	NM_130458	Forward, CCCTTCTCAAGCACCAATGG; reverse, AGGGTGGGTAGTCATTTGCATAG	85
Alp	NM_007431	Forward, CTTGACTGTGGTTACTGCTG; reverse, GAGCGTAATCTACCATGGAG	200
Col1α1	NM_007742	Forward, GGCAAGAATGGAGATGATGG; reverse, CTTAGGACCAGCAGGACCAG	180
Ocn	NM_007541	Forward, CCGGGAGCAGTGTGAGCTTA; reverse, AGGCGGTCTTCAAGCCATACT	69
Gapdh	NM_008084	Forward, GGGTGTGAACCACGAGAAAT; reverse, CCTTCCACAATGCCAAAGTT	120

tissues were sectioned to 4–5 μm and subjected to Alcian blue staining; and poly(methyl methacrylate) sections were subjected to von Kossa staining following standard histology protocols.

To reveal patterning changes in cartilage and bone of the entire skeleton, E18.5 whole embryos of mice were sequentially stained with Alcian blue (for cartilage) and Alizarin red (for bone) as described in previous studies (43). In short, after fixation with 95% ethanol for 48–72 h, embryos were stained with 0.03% (w/v) Alcian blue in 80% ethanol and 20% acetic acid solution for 1–3 days, followed by 0.03% (w/v) Alizarin red in 1% KOH solution for another 12–24 h, and then maintained in a solution of 2% KOH, glycerol (20:80) until analysis.

For immunohistochemistry, deparaffinized sections were antigen-retrived in heated 10 mM citrate buffer (pH 6.0) and then incubated with the primary antibody at 4 °C overnight. On the second day, sections were incubated with appropriate secondary antibodies for 30–60 min at room temperature and developed with 3,3′-diaminobenzidine or 3,3′,5,5′-tetramethylbenzidine as the chromogen following the manufacturer's instructions (Vector Laboratories, Burlingame, CA). After histology or immunohistochemistry, histomorphometric analysis (Bioquant) was performed on tissue sections to quantify the number of positively stained cells per region of interest or per bone surface and the fraction of mineralized bone following the manufacturer's protocols.

RT-PCR, Real Time PCR, and Western Blotting—Total RNA of mouse tissues was extracted using the RNeasy extraction kit (Qiagen), and an equal amount of 1 μg of total RNA per sample was reverse transcribed (first strand RT kit, Fermentas). Regular PCR or quantitative real time PCR (qPCR) was performed using PCR Master Mix (Fermentas) or SYBR Green Supermix (Bio-Rad) with primer sequences listed in Table 1. The level of target gene expression was normalized to the level of the housekeeping gene *Gapdh* (25, 33).

Western blotting was performed as described previously (25, 33). In short, whole cell lysates were assayed for the amount of total cellular protein (Pierce bicinchoninic acid assay, Thermo Scientific, Rockford, IL). Equal loadings of 20-μg aliquots of total protein from each sample were fractionated on 12% Bis-Tris gels following the manufacturer's protocol (Invitrogen). After incubating with appropriate antibodies, immunoreactive bands were visualized with enhanced chemiluminescence (ECL) detection reagents (Amersham Biosciences). The intensities of bands were measured using gel image analysis software (NIH ImageJ_1.32).

Primary Calvaria Culture, Proliferation, and Differentiation Assay—Calvariae were dissected from newborn mice (1–3 days after birth), rinsed with PBS, and digested in freshly made 1 mg/ml collagenase/dispase mixture (Roche Applied Science) in α-Minimal Essential Eagle's Medium at 37 °C for 20 min; the digestion was repeated three times. After digestion, supernatants were combined and centrifuged to pellet cells. Cells were then cultured in α-Minimal Essential Eagle's Medium supplemented with 10% FBS and 1% penicillin/streptomycin (all from Invitrogen). Medium was replaced every 2–3 days. Proliferation of calvaria cells was measured by evaluating cell cycle progression using bromodeoxyuridine (BrdU) incorporation assays (Chemicon, Billerica, MA) according to the manufacturer's instructions.

To induce osteoblast differentiation, calvaria cells were stimulated with rhBMP2 or rhBMP6 at 100 ng/ml for 4 and 7 days. ALP activity and OCN synthesis were evaluated in these cells as markers for immature and mature osteoblasts, respectively. As described previously (25, 33), ALP activity was measured in cell lysates using a colorimetric assay (Sigma) and was normalized to the level of total cellular protein. OCN synthesis was measured in culture medium using a commercially available ELISA kit (Biomedical Technologies, Stoughton, MA).

Serum OCN and Tartrate-resistant Acid Phosphatase Assays—OCN levels in mouse serum were also measured using ELISA kits from Biomedical Technologies. Serum tartrate-resistant acid phosphatase, a marker of bone resorption, was measured using the ELISA-based mouse tartrate-resistant acid phosphatase assay kit from Immunodiagnostic Systems (Fountain Hills, AZ).

Statistical Analysis—Experiments were repeated two to three times independently with five to six samples included in each experimental group. All quantitative measurements are reported as the mean ± S.D. calculated using SigmaPlot8 or Instat statistical software. Differences between two experimental groups were compared by one-way analysis of variance or Student's *t* test with significance accepted at $p < 0.05$.

RESULTS

Bone-specific Deletion of CXCR4 in Osx::CXCR4$^{fl/fl}$ Mice—*Osx*::*CXCR4*$^{fl/fl}$ mice and littermates were genotyped for the presence of *Cre* transgene and floxed *Cxcr4* gene relative to wild type *Cxcr4* (Fig. 1*A*). To validate the *Osx*-controlled *Cxcr4* deletion, we performed RT-PCR to examine *Cxcr4* expression in several tissues derived from newborn *Osx*::*CXCR4*$^{fl/fl}$ mice and Cre-null littermate controls (equivalent to the use of wild type).

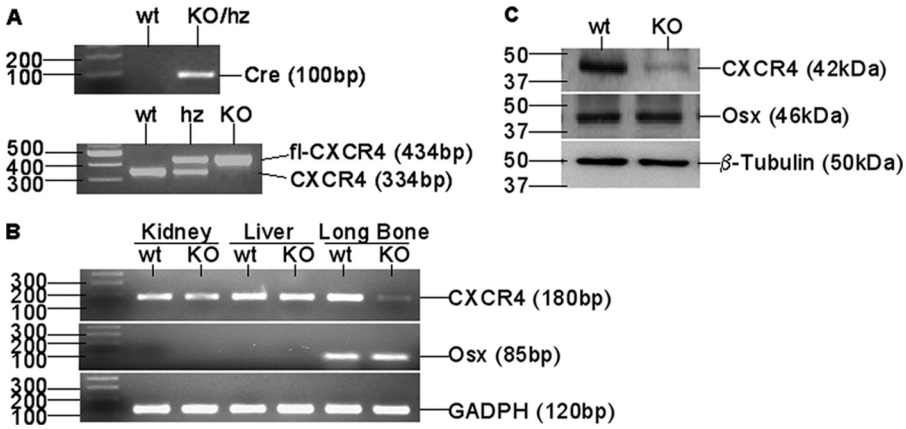

FIGURE 1. **Bone specific-deletion of CXCR4 in *Osx*::*CXCR4*$^{fl/fl}$ mice.** *A*, representative genotyping PCR for *Cre* transgene and floxed (*fl*) *Cxcr4* relative to wild type *Cxcr4* in *Osx*::*CXCR4*$^{fl/fl}$ mice (*KO*), littermates heterozygous (*hz*) for *Cre* and floxed *Cxcr4* (*Osx-Cre*;*CXCR4*$^{fl/+}$), and Cre-null littermates (*CXCR4*$^{fl/+}$ and *CXCR4*$^{fl/fl}$), which were equivalent to wild type (WT) controls. *B*, RT-PCR detection of *Cxcr4*, *Osx*, and *Gapdh* control in kidneys, livers, and long bones (femora and tibiae) derived from newborn (days 1–3 after birth) KO and WT mice. *C*, Western blotting for basal expression of CXCR4, Osx, and β-tubulin control in calvaria cells derived from newborn KO or WT mice. Cells were pooled from $n = 3$ WT or KO mice; experiments were repeated twice using mice from different litters.

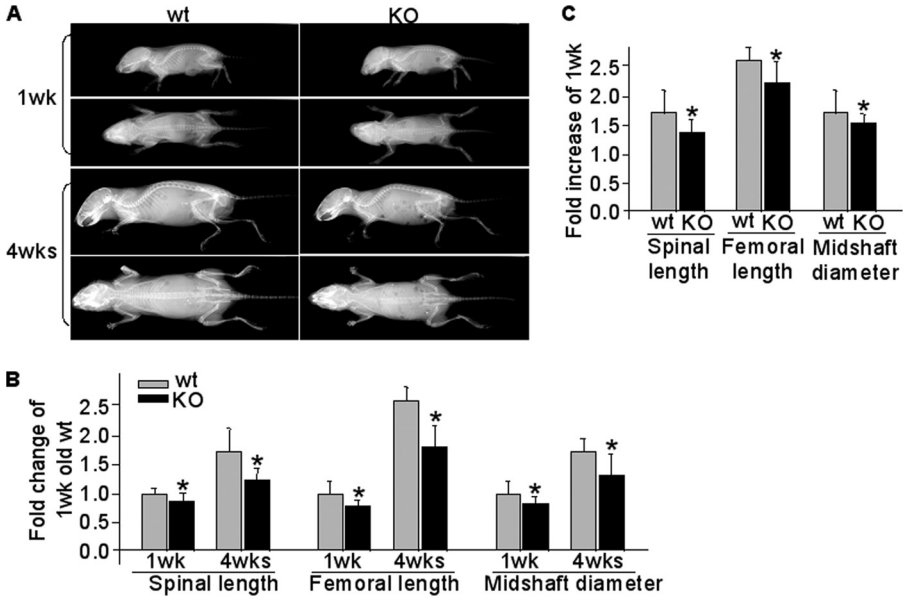

FIGURE 2. **Reduced skeletal size in *Osx*::*CXCR4*$^{fl/fl}$ mice.** *A*, representative x-ray lateral and anterior-posterior view radiographs of *Osx*::*CXCR4*$^{fl/fl}$ (*KO*) mice and Cre-null littermate controls equivalent to WT at 1 and 4 weeks old; all were females. *B*, -fold changes of skeletal size parameters when compared with WT control at 1 week old, which was set as 1. *C*, -fold increases in skeletal size parameters at 4 weeks *versus* those of 1 week in WT or KO mice. $n = 5$ female WT or KO mice at 1 or 4 weeks old. Measurements are presented as mean ± S.D. *, $p < 0.05$ *versus* 1-week-old WT (*B*) or *versus* respective 1-week-old mice (*C*).

When compared with control mice, loss of *Cxcr4* gene was restricted to long bones of *Osx*::*CXCR4*$^{fl/fl}$ mice that expressed *Osx*, whereas no *Cxcr4* deletion relative to the housekeeping gene *Gapdh* was observed in soft organs (kidneys and livers) of *Osx*::*CXCR4*$^{fl/fl}$ mice that did not express *Osx* (Fig. 1*B*).

We also performed Western blotting to compare the protein level of CXCR4 in osteoblastic cells derived from calvariae of newborn *Osx*::*CXCR4*$^{fl/fl}$ mice with that of littermate controls. Osx expression detected in calvaria cells of *Osx*::*CXCR4*$^{fl/fl}$ mice was similar to that of controls; however, reduced CXCR4 expression relative to the β-tubulin control was observed in calvaria osteoblasts of *Osx*::*CXCR4*$^{fl/fl}$ mice *versus* cells of control mice (Fig. 1*C*). Collectively, these data suggest the bone-specific deletion of CXCR4 in *Osx*::*CXCR4*$^{fl/fl}$ mice.

Skeletal Alterations in Osx::CXCR4$^{fl/fl}$ *Mice*—To evaluate the effect of CXCR4 deficiency on the development of mouse skeleton, we compared *Osx*::*CXCR4*$^{fl/fl}$ mice with their sex-matched littermate controls by high resolution x-ray and quantitative μCT. A gross assessment for reduced skeletal size in growing *Osx*::*CXCR4*$^{fl/fl}$ mice *versus* controls was obtained by lateral and anterior-posterior view x-ray radiographs (Fig. 2*A*). When compared with control mice at the same ages, the spinal length of *Osx*::*CXCR4*$^{fl/fl}$ mice was reduced 13% at 1 week and 28% at 4 weeks (Fig. 2*B*). Reduced femoral length (20% at 1 week and 30% at 4 weeks) and femoral midshaft diameter (13% at 1 week and 22% at 4 weeks) were also observed in *Osx*::*CXCR4*$^{fl/fl}$ mice *versus* controls (Fig. 2*B*). Moreover, comparisons between *Osx*::*CXCR4*$^{fl/fl}$ mice and control mice for skeletal growth from 1 to 4 weeks old suggested growth retardation in *Osx*::*CXCR4*$^{fl/fl}$ mice because the increases in spinal length, femoral length, and midshaft diameter were 19, 15, and 14% less, respectively, in *Osx*::*CXCR4*$^{fl/fl}$ mice *versus* controls (Fig. 2*C*).

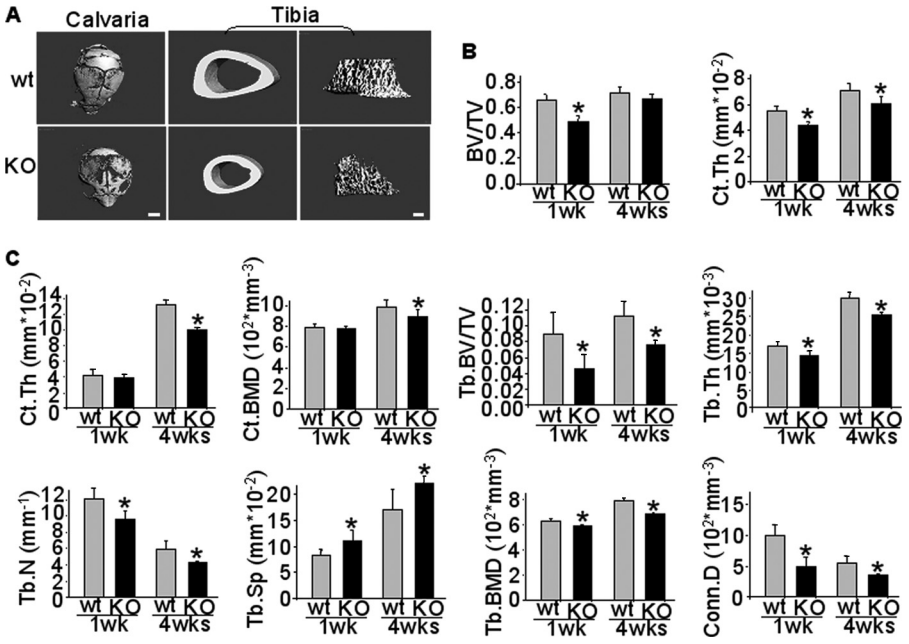

FIGURE 3. **Structural alterations in *Osx*::*CXCR4*$^{fl/fl}$ mice.** *A*, representative μCT images of entire parietal calvariae (1-week-old females) and tibia cortical and trabecular bone (4-week-old females) in *Osx*::*CXCR4*$^{fl/fl}$ mice (*KO*) and Cre-null littermate controls (WT). The *scale bar* equals 1 mm in calvariae or 100 μm in tibiae. *B*, quantitative μCT analysis of calvaria cortical BV/TV and Ct.Th. *C*, quantitative μCT analysis of cortical and trabecular structure on 200 microtomographic slices (2.1 mm) at the proximal tibia. Measurements were Ct.Th, cortical (*Ct.*) BMD, trabecular (*Tb.*) BV/TV, trabecular thickness (*Tb.Th*), trabecular number (*Tb.N*), trabecular separation (*Tb.Sp*), trabecular BMD, and connective tissue density (*Conn.D*). $n = 5$ female WT or KO mice at 1 or 4 weeks old. Measurements are presented as mean $\pm$ S.D. *, $p < 0.05$ *versus* respective WT control.

μCT analysis (Fig. 3, *A*–*C*) further revealed microstructural changes in calvariae and tibiae of *Osx*::*CXCR4*$^{fl/fl}$ mice where bone forms via intramembraneous and endochondral ossification, respectively. When compared with littermate controls at the same ages, a 22% decrease in bone volume fraction (BV/TV) was detected in calvariae of *Osx*::*CXCR4*$^{fl/fl}$ mice at 1 week old, and a slight decrease was observed at 4 weeks (Fig. 3*B*). Cortical thickness (Ct.Th) in calvariae of *Osx*::*CXCR4*$^{fl/fl}$ mice was also reduced at both ages (21% at 1 week and 14% at 4 weeks), suggesting that CXCR4 deficiency results in lower bone mass in calvariae of *Osx*::*CXCR4*$^{fl/fl}$ mice than that of controls (Fig. 3*B*). No significant decrease in bone mineral density (BMD) was detected in calvariae of *Osx*::*CXCR4*$^{fl/fl}$ mice *versus* those of controls at either age (data not shown).

In the proximal tibia, when compared with littermate controls at the same ages, a slightly decreased Ct.Th was observed in 1-week-old *Osx*::*CXCR4*$^{fl/fl}$ mice, and a 24% decrease in Ct.Th was detected in *Osx*::*CXCR4*$^{fl/fl}$ mice at 4 weeks old (Fig. 3*C*). Cortical BMD was also reduced by 11% in tibiae of 4-week-old *Osx*::*CXCR4*$^{fl/fl}$ mice *versus* that of controls (Fig. 3*C*). Cortical porosities (1 − BV/TV) similar to those of littermate controls at both ages were found in tibiae of *Osx*::*CXCR4*$^{fl/fl}$ mice (data not shown).

Markedly decreased trabeculation was detected in the proximal tibia in *Osx*::*CXCR4*$^{fl/fl}$ mice. When compared with littermate controls at both ages, lower BV/TV (44% decrease at 1 week and 32% decrease at 4 weeks), decreased trabecular thickness (18% decrease at 1 week and 17% decrease at 4 weeks), lower numbers of trabeculae (21% decrease at 1 week and 25% decrease at 4 weeks) accompanied by higher trabecular separations (37% increase at 1 week and 30% increase at 4 weeks) were found in tibiae of *Osx*::*CXCR4*$^{fl/fl}$ mice (Fig. 3*C*). Moreover, the trabecular BMD was lower in tibiae of *Osx*::*CXCR4*$^{fl/fl}$ mice at both ages (9% decrease at 1 week and 13% decrease at 4 weeks) as was the connective tissue density of trabeculae (49% decrease at 1 week and 33% decrease at 4 weeks) (Fig. 3*C*). Collectively, these μCT quantitative results were in agreement with qualitative images, suggesting reduced cortical and trabecular bone mass and BMD in endochondral bones of *Osx*::*CXCR4*$^{fl/fl}$ mice.

To determine whether the postnatal skeletal changes originated prenatally, we examined the developing skeletons of E18.5 embryos by sequential Alcian blue and Alizarin red staining. Our data confirmed a smaller size of newborn and E18.5 embryos of *Osx*::*CXCR4*$^{fl/fl}$ mice than that of littermate controls, whereas no significant patterning changes were seen in cartilage or bone in E18.5 embryos of *Osx*::*CXCR4*$^{fl/fl}$ mice (Fig. 4*A*). In addition, we observed less well developed calvariae in E18.5 embryos of *Osx*::*CXCR4*$^{fl/fl}$ mice compared with those of littermate controls as evidenced by a loose mineralized bone structure along with delayed suture closure (Fig. 4*B*). Moreover, when compared with controls, *Osx*::*CXCR4*$^{fl/fl}$ embryos lacked sufficient development of nasal bone around the nasal capsule (Fig. 4*B*). This prenatal calvaria defect correlates to our μCT detections of decreased BV/TV and Ct.Th in postnatal calvariae of *Osx*::*CXCR4*$^{fl/fl}$ mice.

Decreased Bone Mineralization Rate in Osx::CXCR4$^{fl/fl}$ *Mice*—To further understand the effect of CXCR4 deficiency on reducing bone mass and BMD, we compared in *vivo* mineral apposition in *Osx*::*CXCR4*$^{fl/fl}$ mice with their sex-matched littermate controls via double fluorochrome labeling. A smaller distance between xylenol orange- and tetracycline-labeled mineralization fronts at the midshaft of tibia was observed in *Osx*::*CXCR4*$^{fl/fl}$ mice *versus* controls (Fig. 5*A*), suggesting a

lesser amount of new bone formed in *Osx*::*CXCR4*$^{fl/fl}$ mice. Histomorphometric measurements showed that the periosteal MAR of *Osx*::*CXCR4*$^{fl/fl}$ mice was 33% lower than that of littermate controls (Fig. 5*B*).

Decreased mineralization in *Osx*::*CXCR4*$^{fl/fl}$ mice was also suggested by von Kossa staining on the above described fluorochrome-labeled tibiae (Fig. 5*C*). When compared with control mice, we detected a 22% decrease in BV/TV of trabecular bone and a 14% decrease in BV/TV of cortical bone in *Osx*::*CXCR4*$^{fl/fl}$ mice (Fig. 5*D*). These results in combination with our μCT measurements of decreased trabeculation and cortical thickening in tibiae of *Osx*::*CXCR4*$^{fl/fl}$ mice suggest that a lower bone mineralization rate contributes, at least in part, to lower bone mass in these mice.

Growth Plate Disorganization and Abnormal Osteoblast Development in Osx::*CXCR4*$^{fl/fl}$ *Mice*—To understand molecular and cellular changes associated with bone defects in *Osx*::*CXCR4*$^{fl/fl}$ mice, we examined the epiphyseal growth plate where bone formation occurs on a cartilaginous template (44, 45). In both *Osx*::*CXCR4*$^{fl/fl}$ mice and littermate controls, SDF-1 expression was detected mainly in prehypertrophic and hypertrophic chondrocytes and sporadically in bone marrow cells (Fig. 6*A*), and similar numbers of SDF-1-positive cells were found between *Osx*::*CXCR4*$^{fl/fl}$ mice and controls (Fig. 6*B*). In littermate control mice, CXCR4 expression was detected in chondrocytic cells across the proliferative and hypertrophic zones and also continued in the adjacent primary spongiosa by osteoblastic cells and marrow cells (Fig. 6*A*). However, in both regions of *Osx*::*CXCR4*$^{fl/fl}$ mice, CXCR4 expression was markedly reduced (Fig. 6*A*). Histomorphometric analysis showed that, when compared with controls, the number of cells positive for CXCR4 staining was 82% less in a chondrocytic region and 70% less in a region of primary spongiosa in *Osx*::*CXCR4*$^{fl/fl}$ mice (Fig. 6*B*). This pattern of CXCR4 deletion indicated that Osx pro-

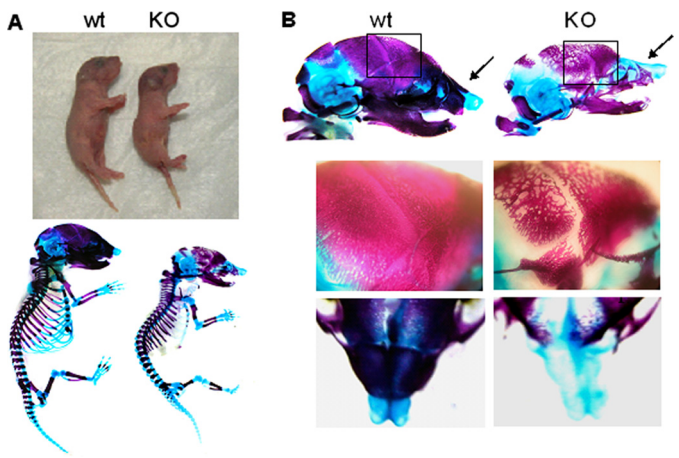

FIGURE 4. **Prenatal skeletal changes in *Osx*::*CXCR4*$^{fl/fl}$ mice.** *A*, representative images of newborn (day 1) *Osx*::*CXCR4*$^{fl/fl}$ mice (*KO*) and Cre-null littermates used as WT controls (*upper panel*) and Alcian blue/Alizarin red staining of E18.5 embryos (*lower panel*). *B*, Alcian blue/Alizarin red staining of entire heads (*upper panel*) and amplified regions of calvaria (*framed areas*) and nose (indicated by *arrows*) of E18.5 embryos (*lower panels*). WT and KO from two different litters were observed.

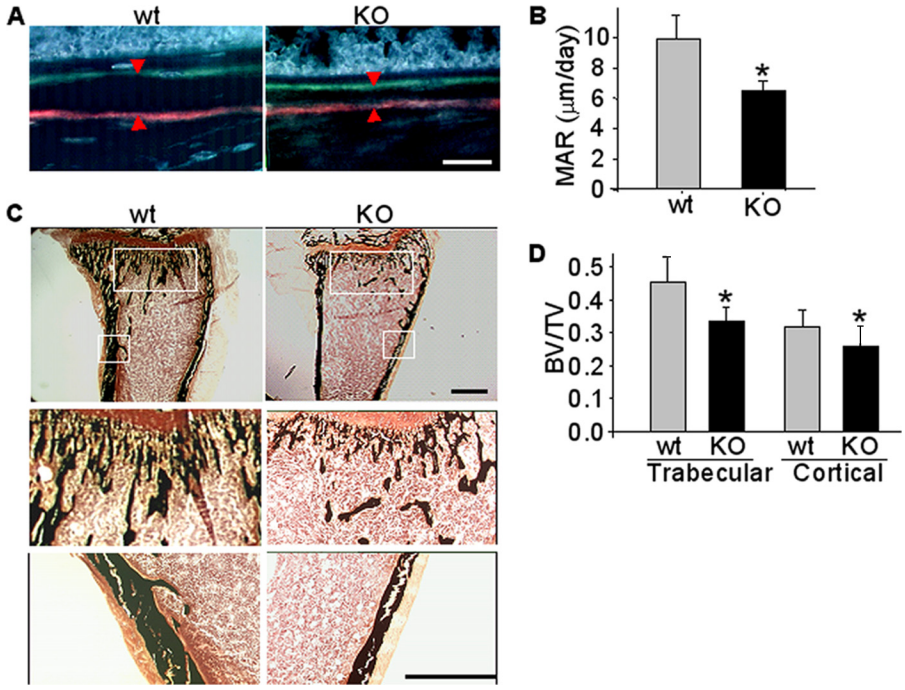

FIGURE 5. **Decreased MAR in *Osx*::*CXCR4*$^{fl/fl}$ mice.** *A*, double fluorochrome-labeling in tibiae of *Osx*::*CXCR4*$^{fl/fl}$ mice (*KO*) and Cre-null littermate controls (WT) by xylenol orange (*orange-red*) and tetracycline (*green*) in a 4-day time interval. The *scale bar* equals 100 μm. *B*, the distance between two fluorochrome-labeled mineralization fronts (indicated by *arrowheads* in *A*) at the midshaft of tibia was quantified using OsteoII software (Bioquant). The MAR was calculated by dividing the measured distance by the time interval. *C*, von Kossa staining of the fluorochrome-labeled tibiae (*upper panel*; *scale bar* equals 500 μm). Mineralized trabecular or cortical bone (amplification of *framed areas*) is stained *black* (*lower panels*; *scale bar* equals 500 μm). *D*, histomorphometric analysis for mineralized bone in von Kossa-stained tibiae. The trabecular BV/TV was determined by dividing the area of mineralized trabecular bone by the total area from the epiphyseal growth plate to the midshaft of tibia. The cortical BV/TV was determined at the midshaft of tibia by dividing the cortical thickness by the total width of tibia. Five measurements per section for three consecutive sections were taken to average each sample. $n = 5$ (females; 2 weeks old) WT or KO mice. Measurements are presented as mean $\pm$ S.D. *, $p < 0.05$ *versus* WT control.

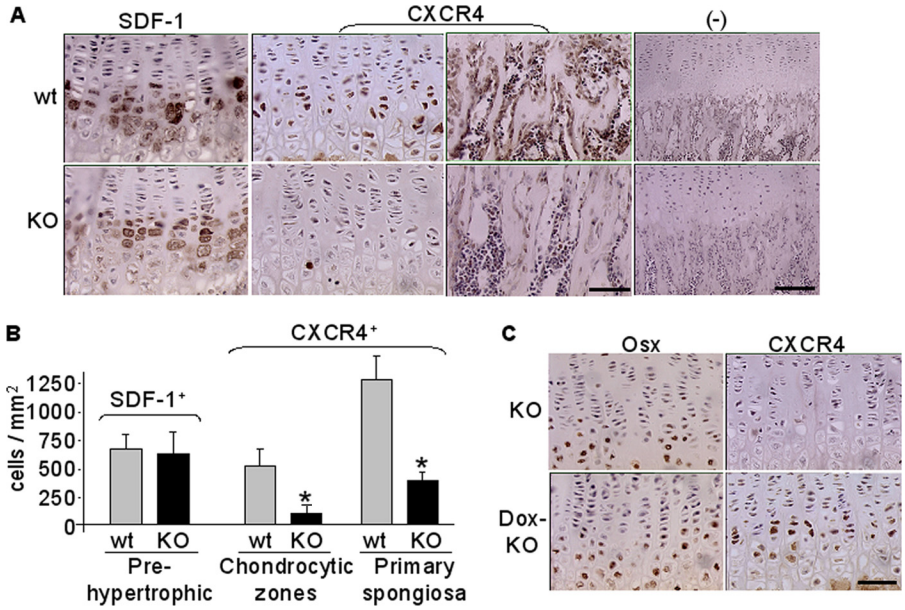

FIGURE 6. **Decreased CXCR4 expression in epiphyseal growth plate of *Osx*::*CXCR4*$^{fl/fl}$ mice (*KO*) *versus* Cre-null littermate controls (WT).** *A*, immunohistochemistry for SDF-1 expression in pre- and hypertrophic chondrocytes and CXCR4 expression in chondrocytic cells and in primary spongiosa (*scale bar* equals 50 μm). Negative (−) controls used isotype-matched control antibodies (*scale bar* equals 100 μm). *B*, histomorphometric analysis (OsteoII software, Bioquant) for the number of cells positive for SDF-1 or CXCR4 expression. The number of cells positive for SDF-1 immunostaining was measured from the pre- to hypertrophic zones. The number of cells positive for CXCR4 was measured in three regions (each at 185 × 250 μm^2) in the middle of the growth plate or the primary spongiosa. Five measurements per section for three consecutive sections were taken to average each sample. *C*, immunohistochemistry for Osx and CXCR4 expression in growth plate of KO mice and control KO mice that were treated with doxycycline (200 μg/ml in drinking water) after birth (*Dox-KO*). $n = 5$ (three females and two males; 4 weeks old) WT or KO mice. Measurements are presented as mean ± S.D. *, $p < 0.05$ *versus* respective WT control.

moter-driven Cre activities occurred not only in osteoblastic cells as expected but also in chondrocytes of *Osx*::*CXCR4*$^{fl/fl}$ mice. In support of this notion, our immunohistochemistry results showed the expression of Osx itself in some chondrocytic cells in the growth plate (Fig. 6*C*). Moreover, in *Osx*::*CXCR4*$^{fl/fl}$ mice that were treated with doxycycline to inactivate the Osx-controlled Cre transcription and recombination (41, 42), we found that CXCR4 loss in chondrocytes was rescued (Fig. 6*C*). No positive staining for SDF-1 or CXCR4 was observed when using isotype-matched control antibodies (Fig. 6*A*). This expression pattern of CXCR4 and SDF-1 implicates a role of SDF-1/CXCR4 signaling in regulating the transition of cartilage to bone.

Next, we examined chondrocyte and osteoblast activities in the growth plate under the influence of CXCR4 deficiency. When compared with littermate controls, as shown by Alcian blue staining, columnar chondrocytes in the proliferative zone of *Osx*::*CXCR4*$^{fl/fl}$ mice appeared to be disorganized with mixed cell size and shape, and no smooth progression in cell size occurred when moving from proliferative to prehypertrophic and hypertrophic zones (Fig. 7*A*). Immunostaining for Col2α1 and Col10α1, specific collagens produced by proliferative and hypertrophic chondrocytes, respectively, further suggested reduced cartilaginous matrix syntheses in *Osx*::*CXCR4*$^{fl/fl}$ mice *versus* controls (Fig. 7*A*). The height of the Col2α1-stained proliferative zone and Col10α1-stained hypertrophic zone was 27 and 23% shorter, respectively, in *Osx*::*CXCR4*$^{fl/fl}$ mice than those of controls (Fig. 7*B*). Moreover, PCNA immunohistochemistry (Fig. 7*A*) indicated reduced proliferation in growth plate chondrocytes as there were 36% fewer cells positive for PCNA staining in *Osx*::*CXCR4*$^{fl/fl}$ mice compared with controls (Fig. 7*C*). These observations suggest that reduced proliferation and size of a cartilaginous template in *Osx*::*CXCR4*$^{fl/fl}$ mice correlate to the reduced long bone size in these mice.

CXCR4 deficiency also affected osteoblast activities in the primary spongiosa where osteoblasts differentiate and lay down new bone matrix on the hypertrophic chondrocyte residues (44, 45). Our immunohistochemistry showed strong Osx expression in osteoblastic cells of the primary spongiosa in both *Osx*::*CXCR4*$^{fl/fl}$ and control mice (Fig. 8*A*), and no significant difference in the number of Osx-expressing cells was observed between *Osx*::*CXCR4*$^{fl/fl}$ mice and controls (Fig. 8*B*). We further detected the expression of ProCol1α1, a marker of initial collagen synthesis in relatively mature osteoblastic cells, along with OCN, a protein typically synthesized by mature osteoblasts, in the primary spongiosa by osteoblastic cells lining the trabecular bone surfaces (Fig. 8*A*). However, histomorphometric analysis showed that the number of cells positively stained for ProCol1α1 and OCN per bone surface was 62 and 56% less, respectively, in *Osx*::*CXCR4*$^{fl/fl}$ mice than that of controls (Fig. 8*B*). This suggests an arrested osteoblast progression toward mature osteoblasts in the growth plate of *Osx*::*CXCR4*$^{fl/fl}$ mice.

Additional evidence for impaired osteoblast development was obtained in long bones derived from newborn *Osx*::*CXCR4*$^{fl/fl}$ mice that showed reduced *Cxcr4* expression compared with that of littermate controls (Fig. 1*B*). Our RT-PCR results revealed similar *Osx* expression but reduced *Col1α1* and *Ocn* expression in bones of *Osx*::*CXCR4*$^{fl/fl}$ mice *versus* those of controls (Fig. 8*C*). Moreover, qPCR analysis showed that the level of *Col1α1* and *Ocn* expression relative to

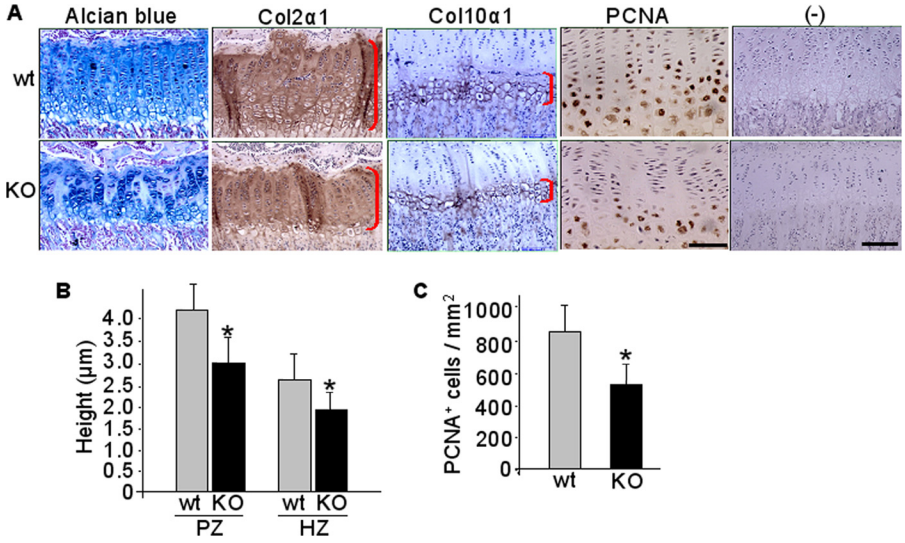

FIGURE 7. **Epiphyseal growth plate disorganization in tibiae of *Osx*::*CXCR4*$^{fl/fl}$ mice.** *A*, representative Alcian blue staining; immunohistochemistry for Col2α1, Col10α1, and PCNA; and negative (−) controls using isotype-matched control antibody. The *scale bar* equals 50 μm in PCNA-stained sections or 100 μm in the rest of the sections. *B*, histomorphometric analysis (OsteoII, Bioquant) for the height of the proliferative (*PZ*) and hypertrophic zones (*HZ*) in the middle of the growth plate (indicated by *right brackets* in *A*). *C*, histomorphometric measurements for the number of PCNA-stained cells from the proliferative to hypertrophic zones. Five measurements per section for three consecutive sections were taken to average each sample. $n = 5$ (three females and two males; 4 weeks old) WT or KO mice. Measurements are presented as mean ± S.D. *, $p < 0.05$ *versus* WT control.

Gapdh control was reduced by 74 and 68%, respectively, in bone of *Osx*::*CXCR4*$^{fl/fl}$ mice compared with control mice, whereas no significant decrease was detected in the level of *Osx* expression in *Osx*::*CXCR4*$^{fl/fl}$ bones (Fig. 8*D*). Consistent with decreased gene expression of *Ocn* in bone, a 17% reduction in the serum level of OCN was further detected in adult *Osx*::*CXCR4*$^{fl/fl}$ mice when compared with control mice (Fig. 8*E*), whereas no significant increase in the serum level of tartrate-resistant acid phosphatase was found in *Osx*::*CXCR4*$^{fl/fl}$ mice (data not shown). Taken together, these findings suggest that lower bone mass in *Osx*::*CXCR4*$^{fl/fl}$ mice was associated with decreased bone formation via impaired osteoblast development.

CXCR4 Deficiency Inhibited Cell Proliferation and Impaired BMP-induced Osteoblast Differentiation—To gain further insights into the function of CXCR4 in osteoblast activities, we examined calvaria cells derived from newborn *Osx*::*CXCR4*$^{fl/fl}$ mice (proved to be CXCR4-deficient; Fig. 1*C*) and littermate controls for cell proliferation and differentiation in response to BMP stimulation. A 43% lower BrdU incorporation was detected in cells of *Osx*::*CXCR4*$^{fl/fl}$ mice *versus* cells of control mice, suggesting a lower proliferation rate in CXCR4-deficient osteoblasts (Fig. 9*A*). Moreover, similar to our detection of arrested osteoblast progression in long bones, a 32% lower level of *Alp* expression and a 70% lower level of *Ocn* expression relative to *Gapdh* control were detected in calvaria cells of *Osx*::*CXCR4*$^{fl/fl}$ mice *versus* cells of control mice (Fig. 9*B*). After stimulation with BMP2, a member of the BMP family, in calvaria cells of control mice, both levels of ALP activity (Fig. 9*C*) and OCN synthesis (Fig. 9*D*) were significantly increased (2.4-fold for ALP at day 4 and 4-fold for OCN at day 7) over base-line levels in cultures maintained in medium only. In contrast, there was no increase in either ALP (Fig. 9*C*) or OCN (Fig. 9*D*) in BMP2-stimulated calvaria cells of *Osx*::*CXCR4*$^{fl/fl}$ mice *versus* medium-only controls. Similarly, stimulation with BMP6, another member of the BMP family, significantly increased the level of ALP (1.8-fold at day 4) and OCN (2.5-fold at day 7) in calvaria cells of control mice, whereas no response to BMP6 stimulation was detected in calvaria cells of *Osx*::*CXCR4*$^{fl/fl}$ mice (Fig. 9, *E* and *F*). These data suggest that CXCR4 deficiency inhibits osteoblastic differentiation of calvaria cells induced by two members of the BMP family.

Our Western blotting results further showed impaired BMP signaling cascades in CXCR4-deficient calvaria cells (Fig. 10, *A* and *B*). Although BMP2 stimulation rapidly induced phosphorylation of intracellular R-Smads (Smad1/5/8) and Erk1/2, the key downstream targets of BMP signal transduction, in calvaria cells derived from control mice, no BMP2-stimulated phosphorylations of R-Smads and Erk were observed in CXCR4-deficient calvaria cells derived from *Osx*::*CXCR4*$^{fl/fl}$ mice (Fig. 10*A*). Gel image analysis showed that, when compared with medium-only control cells, the intensities of immunoreactive bands for phosphorylated (p) Smad1/5 and pErk1/2 were increased 5- and 4-fold, respectively, in BMP2-stimulated calvaria cells derived from control mice; in contrast, no significant increases in band intensities of pSmad1/5 and pErk1/2 after BMP2 stimulation were detected in calvaria cells of *Osx*::*CXCR4*$^{fl/fl}$ mice (Fig. 10*B*).

Moreover, we compared *Osx*::*CXCR4*$^{fl/fl}$ mice with control mice for Smad1/5 phosphorylation in both calvaria (Fig. 10*C*) and the epiphyseal growth plate (Fig. 10*D*) by immunohistochemistry. In calvariae, the number of cells positive for pSmad1/5 staining was reduced by 72% in *Osx*::*CXCR4*$^{fl/fl}$ mice *versus* controls (Fig. 10*E*). In tibiae, pSmad1/5 expression was detected in pre- and hypertrophic chondrocytes in the growth plate (Fig. 10*D*), where the number of cells expressing pSmad1/5 was reduced by 76% in *Osx*::*CXCR4*$^{fl/fl}$ mice when compared with that of control mice (Fig. 10*E*). Other than BMP-regulated Smads, we also examined Smad2,

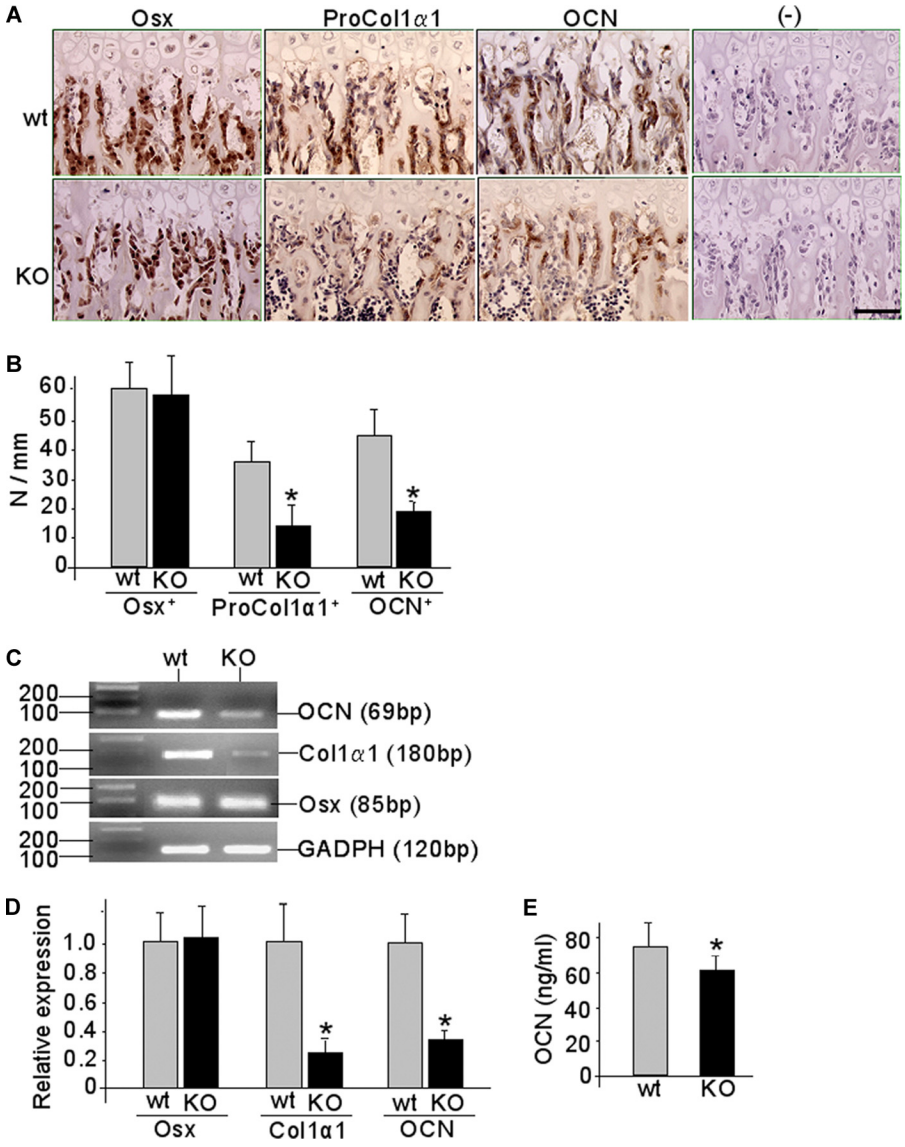

FIGURE 8. **Arrested osteoblast progression in *Osx*::*CXCR4*$^{fl/fl}$ mice.** *A*, representative immunohistochemistry for Osx, ProCol1α1, and OCN in the primary spongiosa of *Osx*::*CXCR4*$^{fl/fl}$ (*KO*) mice and Cre-null littermate controls (WT). Isotype-matched control IgGs were used in negative (−) controls. The *scale bar* equals 50 μm. *B*, histomorphometric analysis (OsteoII, Bioquant) for the number of positively stained cells per bone surface in three regions (each at 185 × 250 μm^2) in the middle of the primary spongiosa. Five measurements per section for three consecutive sections were taken to average each sample. $n = 5$ (three females and two males; 4 weeks old) WT or KO mice. *C*, representative RT-PCR detection for *Osx*, *Col1α1*, *Ocn*, and *Gapdh* control in long bones derived from newborn (days 1–3 after birth) KO or WT mice. *D*, qPCR quantification of the expression level of *Osx*, *Col1α1*, and *Ocn* relative to *Gapdh* control in long bones derived from newborn KO or WT mice. $n = 5$ WT or KO. *E*, serum OCN level in KO mouse *versus* WT controls. $n = 5$ (three females and two males; 12 weeks old). All measurements are presented as mean ± S.D. *, $p < 0.05$ *versus* WT control.

a key intracellular transducer for TGFβ1/2/3 signaling, in the growth plate. Our data showed weak pSmad2 expression in *Osx*::*CXCR4*$^{fl/fl}$ mice similar to that in control mice (Fig. 10*D*), confirming the specific involvement of BMP signaling rather than other members of the TGFβ superfamily in this case. Collectively, these data showed impaired BMP signaling in CXCR4-deficient cells and bone tissues, and thus suggest that CXCR4 functions in regulating osteoblast activities in cooperation with BMP signaling.

DISCUSSION

The current literature illustrates multiple functions of CXCR4 in embryonic organ development, HIV and tumor invasion, and various tissue homeostasis and repair processes that require the chemotactic interaction of CXCR4 with its ligand, SDF-1 (1–7, 9–16). However, it remains unknown whether CXCR4 has a direct functional role in bone formation. In this study, we addressed this question by demonstrating the effect of bone-specific deletion of CXCR4 on postnatal skeletal development of the mouse and identified the function of CXCR4 in regulating osteoblast development. This finding enhances the current understanding of CXCR4 with a novel concept that CXCR4, the essential signaling component for SDF-1, is required for proper bone formation.

Via the transcriptional control of Osx, we were able to target CXCR4 deletion in osteoprecursor cells and thus focused on analyzing the role of CXCR4 during bone formation. However, we noticed that CXCR4 was not completely

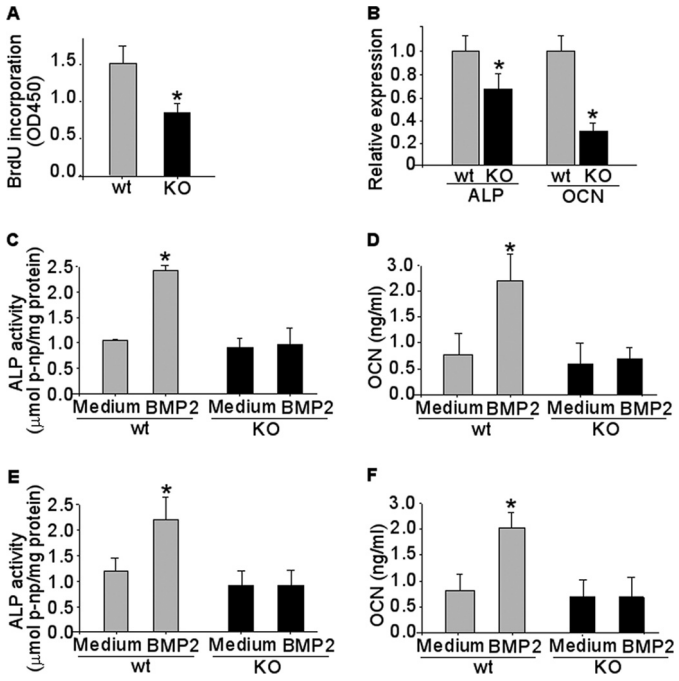

FIGURE 9. **CXCR4 deficiency inhibits cell proliferation and osteoblast differentiation induced by BMP.** Primary osteoblastic cells were derived from newborn (days 1–3 after birth) calvariae of *Osx*::*CXCR4*$^{fl/fl}$ (*KO*) mice and Cre-null littermate controls (WT). *A*, BrdU incorporation for 6 h in WT or KO calvaria cells. *B*, qPCR measurements of base-line mRNA levels of *Alp* and *Ocn* relative to *Gapdh* control in calvaria cells of WT or KO mice. *C–F*, calvaria cells were stimulated with rhBMP2 (*C* and *D*) or rhBMP6 (*E* and *F*) protein at 100 ng/ml for 4 or 7 days or were maintained in culture medium without any stimulation as controls. ALP activities were measured in cell lysates and normalized to the level of total cellular protein. OCN levels were measured in cell medium using ELISA. Cultures were pooled from calvariae of $n = 3$ WT or KO mice, and triplicate wells of cells were used for each sample. Experiments were repeated twice using mice from two different litters. Measurements are expressed as mean ± S.D. *, $p < 0.05$ *versus* respective medium-only control.

removed with this approach as evidenced by trace CXCR4 expression remaining in the Osx-expressing cells and bones (Fig. 1, *B* and *C*). This might have lessened the severity of bone defects in *Osx*::*CXCR4*$^{fl/fl}$ mice resulting from CXCR4 deficiency. Although Osx is considered as one of the osteoblastic lineage-specific transcription factors, we observed CXCR4 deletion in both osteoblasts and growth plate chondrocytes of *Osx*::*CXCR4*$^{fl/fl}$ mice (Fig. 6, *A–C*), suggesting that broader Cre activities occurred in both osteoblastic and chondrocytic cells. We further verified this point by shutting down the Osx-driven Cre activity with doxycycline administration, which restored CXCR4 expression in chondrocytes of *Osx*::*CXCR4*$^{fl/fl}$ mice (Fig. 6*C*). In agreement with our findings, several previous studies also reported Osx expression in chondrocytes (35, 46). Moreover, when using R26LacZ reporter mice, the Osx-controlled Cre activity was originally noticed in chondrocytic cells in the Osx-Cre strain (41, 42). Similar to previous findings of CXCR4 and SDF-1 expression in the growth plate of a long bone (26, 28, 47), we also detected their expression in the growth plate of Cre-null littermate controls for *Osx*::*CXCR4*$^{fl/fl}$ mice. The pattern of CXCR4 expression in the growth plate and adjacent primary spongiosa and SDF-1 expression in pre- and hypertrophic chondrocytes at the chondro-osseous junction indicates that SDF-1 may function in both chondrocytes and osteoblasts via signaling through CXCR4. Moreover, this pattern of SDF-1 expression may serve to recruit CXCR4-expressing progenitor cells at blood vessel invasion to lay down new bone on the hypertrophic chondrocyte residues. Our detection of SDF-1 expression pattern in 4-week-old mice is different from that reported by Wei *et al.* (34) in newborn (day 1) mice in which SDF-1 was predominantly expressed in bone marrow next to hypertrophic chondrocytes, suggesting an age-related change in cellular distribution of SDF-1 that may be associated with SDF-1 function at different stages of bone development. This hypothesis remains to be tested.

A growth plate controls the size and shape of a long bone; therefore, a shorter cartilaginous template with decreased chondrocyte proliferation and collagen matrix synthesis in the growth plate of *Osx*::*CXCR4*$^{fl/fl}$ mice correlates to the reduced long bone size in these mice. Lower BMD and reduced cortical thickness and trabecular bone volume in tibiae of *Osx*::*CXCR4*$^{fl/fl}$ mice (Fig. 3, *A–C*) suggest that CXCR4 is required as an endogenous regulator for skeletal size and bone architecture. Moreover, a slower bone mineralization rate (Fig. 5, *A–B*) further correlates to growth retardation in the skeletal development of *Osx*::*CXCR4*$^{fl/fl}$ mice (Fig. 2*C*). Although we also detected decreased bone mass in calvariae of *Osx*::*CXCR4*$^{fl/fl}$ mice, their BMD was not significantly reduced as we found in tibiae. This suggests differential roles of CXCR4 in intramembranous and endochondral ossification alone or via interacting with other signaling pathways that participate in these processes. When looking into mechanisms underlying bone defects in *Osx*::*CXCR4*$^{fl/fl}$ mice, we identified reduced Col1α1 and OCN expression relative to unreduced Osx expression in osteoblastic cells adjacent to growth plate (Fig. 8, *A* and *B*), suggesting an arrested osteoblast progression toward mature osteoblasts in these mice. Concomitantly, a lesser expression of mature osteoblast markers was found in long bones of newborn mice and serum of adult mice (Fig. 8, *C–E*). Taken together, these findings suggest that arrested osteoblast development contributes, at least in part, to the reduced bone formation in *Osx*::*CXCR4*$^{fl/fl}$ mice.

Decreased proliferation and a blunted response to BMP2 or BMP6 osteoblast differentiation in primary calvaria cells of *Osx*::*CXCR4*$^{fl/fl}$ mice add additional evidence to CXCR4 function in osteoblast activities. The findings that CXCR4-deficienct cells did not express sufficient levels of ALP activities and did not adequately synthesize OCN protein after BMP stimulation (Fig. 9, *C–F*) are consistent with our previous detections in cultures for bone marrow stromal cells and C2C12 and ST2 cells, where blocking SDF-1/CXCR4 by siRNA, antibody, or antagonist against SDF-1 or CXCR4 inhibits the BMP2-induced cell differentiation toward the osteoblast lineage (25, 33). Moreover, suppressed BMP signaling cascades were detected in calvaria-derived cells as well as in CXCR4-deficient long bones and calvariae of *Osx*::*CXCR4*$^{fl/fl}$ mice (Fig. 10, *A–E*). Furthermore, no suppression of pSmad2 in CXCR4-deficient tibiae excluded the involvement of other members of the TGFβ superfamily. These findings demonstrated an *in vivo* interaction between

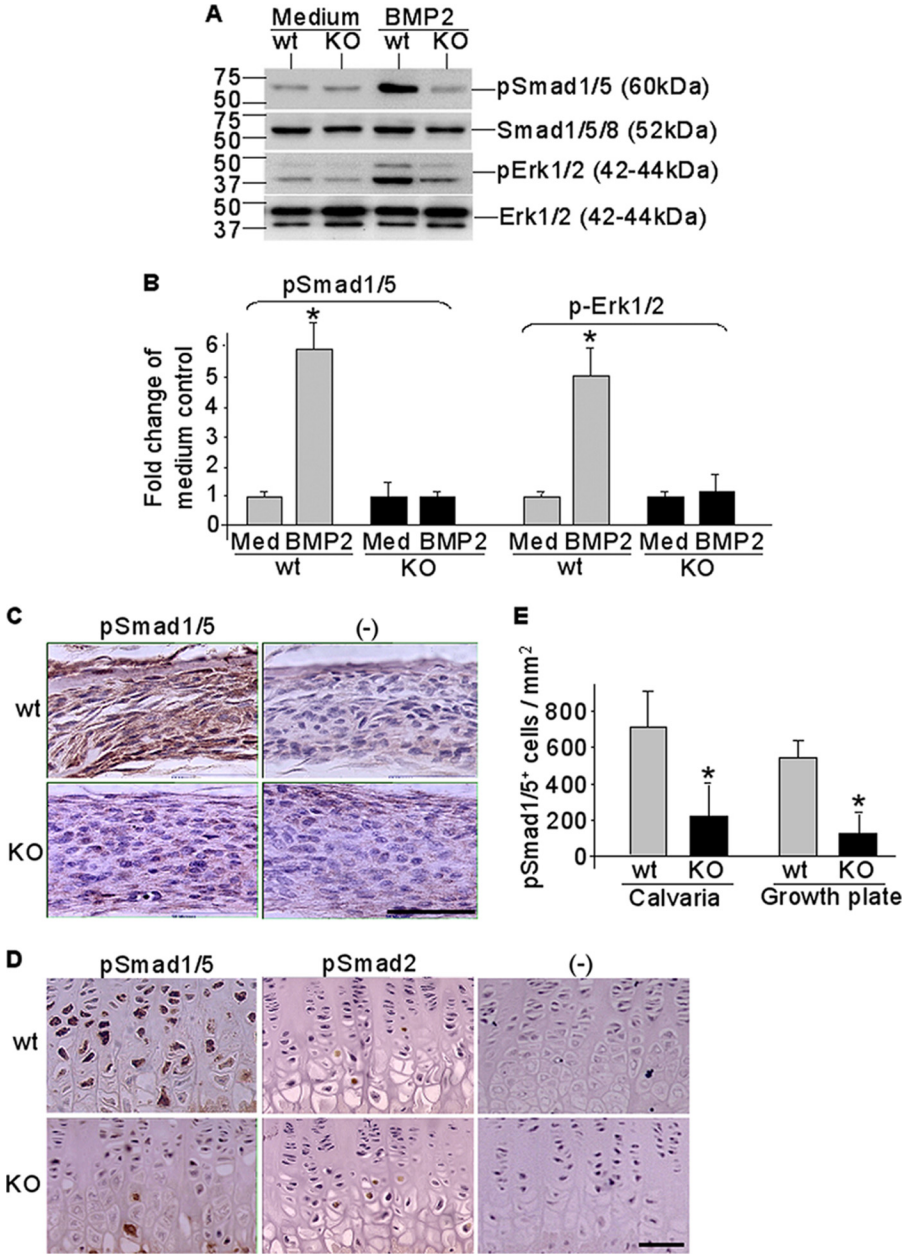

FIGURE 10. **Impaired BMP signaling in CXCR4-deficient cells and bone tissues.** Calvaria osteoblasts were derived from newborn (days 1–3 after birth) *Osx*::*CXCR4*$^{fl/fl}$ (*KO*) mice or Cre-null littermate controls (WT). Cells were stimulated with rhBMP2 at 100 ng/ml for 15 min or were maintained in culture medium (*Med*) only as controls. *A* and *B*, Western detection of Smad1/5 and Erk1/2 phosphorylation relative to unphosphorylated total Smads and Erk (*A*) and gel image analysis for band intensities of pSmad1/5 and pErk1/2 compared with that of medium-only control cells (*B*). Cultures were pooled from calvariae of $n = 3$ WT or KO mice, and triplicate wells of cells were used for each sample. Experiments were repeated twice using mice from two different litters. Measurements are expressed as mean ± S.D. *, $p < 0.05$ *versus* respective medium-only control. *C–E*, immunohistochemistry detection of pSmad1/5 expression in calvaria (*C*) and pSmad1/5 and pSmad2 expression in tibia growth plate (*D*) followed by histomorphometric analysis (OsteoII, Bioquant) for the number of positively stained cells in three regions of calvaria (each at 185 × 250 μm^2) and from the pre- to hypertrophic zones in the growth plate of tibia (*E*). Isotype-matched control IgGs were used in negative (−) controls. The *scale bar* equals 50 μm in calvaria or growth plate sections. Five measurements per section for three consecutive sections were taken to average each sample. $n = 5$ (three females and two males; 4 weeks old) WT or KO. All measurements are expressed as mean ± S.D. *, $p <$ 0.05 *versus* respective WT control.

CXCR4 and BMP in bone and suggest that CXCR4 regulates osteoblast development in postnatal bone formation involving its cooperation with BMP signaling. Future studies are required to determine the roles of different members of the BMP family in CXCR4-regulated bone formation.

In conclusion, our data suggest that loss of *Cxcr4* gene in the *Osx*-expressing osteoprecursors results in impaired bone development and growth in the mouse skeleton, and this is associated with the regulation of CXCR4 in osteoblast development. These findings established a direct functional role of CXCR4 in bone formation *in vivo*. Targeting the SDF-1/CXCR4 pathway will deepen our understanding of the molecular regulation of osteogenesis and will help to develop new therapeutic targets to treat defective bone formation and regeneration ranging from metabolic bone diseases to fracture non-unions.

Acknowledgment—We thank Dr. Yong-Rui Zou at Columbia University for kindly providing CXCR4$^{fl/fl}$ mice.

REFERENCES

1. Shirozu, M., Nakano, T., Inazawa, J., Tashiro, K., Tada, H., Shinohara, T., and Honjo, T. (1995) *Genomics* **28,** 495–500
2. D'Apuzzo, M., Rolink, A., Loetscher, M., Hoxie, J. A., Clark-Lewis, I., Melchers, F., Baggiolini, M., and Moser, B. (1997) *Eur. J. Immunol.* **27,** 1788–1793
3. Yu, L., Cecil, J., Peng, S. B., Schrementi, J., Kovacevic, S., Paul, D., Su, E. W., and Wang, J. (2006) *Gene* **374,** 174–179
4. Zlotnik, A., and Yoshie, O. (2000) *Immunity* **12,** 121–127
5. Nagasawa, T., Hirota, S., Tachibana, K., Takakura, N., Nishikawa, S., Kitamura, Y., Yoshida, N., Kikutani, H., and Kishimoto, T. (1996) *Nature* **382,** 635–638
6. Ma, Q., Jones, D., Borghesani, P. R., Segal, R. A., Nagasawa, T., Kishimoto, T., Bronson, R. T., and Springer, T. A. (1998) *Proc. Natl. Acad. Sci. U.S.A.* **95,** 9448–9453
7. Zou, Y. R., Kottmann, A. H., Kuroda, M., Taniuchi, I., and Littman, D. R. (1998) *Nature* **393,** 595–599
8. Diaz, G. A. (2005) *Immunol. Rev.* **203,** 235–243
9. Baggiolini, M. (1998) *Nature* **392,** 565–568
10. Aiuti, A., Tavian, M., Cipponi, A., Ficara, F., Zappone, E., Hoxie, J., Peault, B., and Bordignon, C. (1999) *Eur. J. Immunol.* **29,** 1823–1831
11. Yu, X., Huang, Y., Collin-Osdoby, P., and Osdoby, P. (2003) *J. Bone Miner. Res.* **18,** 1404–1418
12. Dar, A., Kollet, O., and Lapidot, T. (2006) *Exp. Hematol.* **34,** 967–975
13. Gronthos, S., Simmons, P. J., Graves, S. E., and Robey, P. G. (2001) *Bone* **28,** 174–181
14. Peled, A., Kollet, O., Ponomaryov, T., Petit, I., Franitza, S., Grabovsky, V., Slav, M. M., Nagler, A., Lider, O., Alon, R., Zipori, D., and Lapidot, T. (2000) *Blood* **95,** 3289–3296
15. Kitaori, T., Ito, H., Schwarz, E. M., Tsutsumi, R., Yoshitomi, H., Oishi, S., Nakano, M., Fujii, N., Nagasawa, T., and Nakamura, T. (2009) *Arthritis Rheum.* **60,** 813–823
16. Otsuru, S., Tamai, K., Yamazaki, T., Yoshikawa, H., and Kaneda, Y. (2008) *Stem Cells* **26,** 223–234
17. Lataillade, J. J., Clay, D., Dupuy, C., Rigal, S., Jasmin, C., Bourin, P., and Le Bousse-Kerdilès, M. C. (2000) *Blood* **95,** 756–768
18. Majka, M., Ratajczak, J., Lee, B., Honczarenko, M., Douglas, R., Kowalska, M. A., Silberstein, L., Gewirtz, A. M., and Ratajczak, M. Z. (2000) *Stem Cells* **18,** 128–138
19. Ji, J. F., He, B. P., Dheen, S. T., and Tay, S. S. (2004) *Stem Cells* **22,** 415–427
20. Hill, W. D., Hess, D. C., Martin-Studdard, A., Carothers, J. J., Zheng, J., Hale, D., Maeda, M., Fagan, S. C., Carroll, J. E., and Conway, S. J. (2004) *J. Neuropathol. Exp. Neurol.* **63,** 84–96
21. Ratajczak, M. Z., Majka, M., Kucia, M., Drukala, J., Pietrzkowski, Z., Peiper, S., and Janowska-Wieczorek, A. (2003) *Stem Cells* **21,** 363–371
22. Hatch, H. M., Zheng, D., Jorgensen, M. L., and Petersen, B. E. (2002) *Cloning Stem Cells* **4,** 339–351
23. Tögel, F., Isaac, J., Hu, Z., Weiss, K., and Westenfelder, C. (2005) *Kidney Int.* **67,** 1772–1784
24. Ceradini, D. J., Kulkarni, A. R., Callaghan, M. J., Tepper, O. M., Bastidas, N., Kleinman, M. E., Capla, J. M., Galiano, R. D., Levine, J. P., and Gurtner, G. C. (2004) *Nat. Med.* **10,** 858–864
25. Zhu, W., Boachie-Adjei, O., Rawlins, B. A., Frenkel, B., Boskey, A. L., Ivashkiv, L. B., and Blobel, C. P. (2007) *J. Biol. Chem.* **282,** 18676–18685
26. Sun, Y. X., Schneider, A., Jung, Y., Wang, J., Dai, J., Wang, J., Cook, K., Osman, N. I., Koh-Paige, A. J., Shim, H., Pienta, K. J., Keller, E. T., McCauley, L. K., and Taichman, R. S. (2005) *J. Bone Miner. Res.* **20,** 318–329
27. Kortesidis, A., Zannettino, A., Isenmann, S., Shi, S., Lapidot, T., and Gronthos, S. (2005) *Blood* **105,** 3793–3801
28. Jung, Y., Wang, J., Schneider, A., Sun, Y. X., Koh-Paige, A. J., Osman, N. I., McCauley, L. K., and Taichman, R. S. (2006) *Bone* **38,** 497–508
29. Salvucci, O., Yao, L., Villalba, S., Sajewicz, A., Pittaluga, S., and Tosato, G. (2002) *Blood* **99,** 2703–2711
30. Petit, I., Szyper-Kravitz, M., Nagler, A., Lahav, M., Peled, A., Habler, L., Ponomaryov, T., Taichman, R. S., Arenzana-Seisdedos, F., Fujii, N., Sandbank, J., Zipori, D., and Lapidot, T. (2002) *Nat. Immunol.* **3,** 687–694
31. Ponomaryov, T., Peled, A., Petit, I., Taichman, R. S., Habler, L., Sandbank, J., Arenzana-Seisdedos, F., Magerus, A., Caruz, A., Fujii, N., Nagler, A., Lahav, M., Szyper-Kravitz, M., Zipori, D., and Lapidot, T. (2000) *J. Clin. Investig.* **106,** 1331–1339
32. Wynn, R. F., Hart, C. A., Corradi-Perini, C., O'Neill, L., Evans, C. A., Wraith, J. E., Fairbairn, L. J., and Bellantuono, I. (2004) *Blood* **104,** 2643–2645
33. Hosogane, N., Huang, Z., Rawlins, B. A., Liu, X., Boachie-Adjei, O., Boskey, A. L., and Zhu, W. (2010) *Int. J. Biochem. Cell Biol.* **42,** 1132–1141
34. Wei, L., Kanbe, K., Lee, M., Wei, X., Pei, M., Sun, X., Terek, R., and Chen, Q. (2010) *Dev. Biol.* **341,** 236–245
35. Nakashima, K., Zhou, X., Kunkel, G., Zhang, Z., Deng, J. M., Behringer, R. R., and de Crombrugghe, B. (2002) *Cell* **108,** 17–29
36. Ducy, P., Zhang, R., Geoffroy, V., Ridall, A. L., and Karsenty, G. (1997) *Cell* **89,** 747–754
37. Otto, F., Thornell, A. P., Crompton, T., Denzel, A., Gilmour, K. C., Rosewell, I. R., Stamp, G. W., Beddington, R. S., Mundlos, S., Olsen, B. R., Selby, P. B., and Owen, M. J. (1997) *Cell* **89,** 765–771
38. Nie, Y., Waite, J., Brewer, F., Sunshine, M. J., Littman, D. R., and Zou, Y. R. (2004) *J. Exp. Med.* **200,** 1145–1156
39. Nie, Y., Han, Y. C., and Zou, Y. R. (2008) *J. Exp. Med.* **205,** 777–783
40. Agarwal, U., Ghalayini, W., Dong, F., Weber, K., Zou, Y. R., Rabbany, S. Y., Rafii, S., and Penn, M. S. (2010) *Circ. Res.* **107,** 667–676
41. Rodda, S. J., and McMahon, A. P. (2006) *Development* **133,** 3231–3244
42. Berman, S. D., Calo, E., Landman, A. S., Danielian, P. S., Miller, E. S., West, J. C., Fonhoue, B. D., Caron, A., Bronson, R., Bouxsein, M. L., Mukherjee, S., and Lees, J. A. (2008) *Proc. Natl. Acad. Sci. U.S.A.* **105,** 11851–11856
43. McLeod, M. J. (1980) *Teratology* **22,** 299–301
44. Kronenberg, H. M. (2003) *Nature* **423,** 332–336
45. Karsenty, G. (2003) *Nature* **423,** 316–318
46. Koyama, E., Young, B., Nagayama, M., Shibukawa, Y., Enomoto-Iwamoto, M., Iwamoto, M., Maeda, Y., Lanske, B., Song, B., Serra, R., and Pacifici, M. (2007) *Development* **134,** 2159–2169
47. Wang, Y., Zhang, M., Middleton, F. A., Horton, J. A., Pritchard, M., Spadaro, J. A., Farnum, C. E., and Damron, T. A. (2007) *Cells Tissues Organs* **186,** 192–203